Analyst

Accepted Manuscript

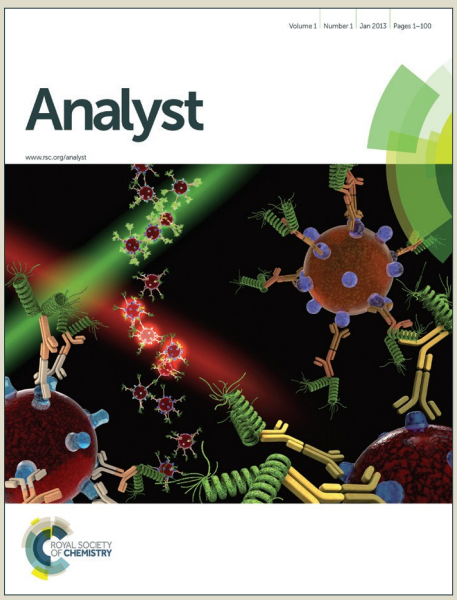

ROYAL SOCIETY OF CHEMISTRY

www.rsc.org/analyst

A Two-Phase Approach to Fourier Transform Ion Mobility Time-of-Flight Mass Spectrometry

Brian H. Clowers[a], William F. Siems, Zhihao Yu, Austen L. Davis

Department of Chemistry
Washington State University
Pullman, WA 99164, USA

[a] Corresponding Author: Brian H. Clowers
e-mail: brian.clowers@wsu.edu
Tel: 509-335-4300

Abstract

It is well known that the duty cycle of common drift-tube ion mobility experiments is often below 1%. However, multiplexing approaches such as Fourier and Hadamard pulsing schemes have been shown to independently enhance the throughput of ion mobility spectrometry (IMS) experiments to levels that approach 50%. While challenges remain to their broad scale implementation we describe a new Fourier transform (FT) IMS experiment that is directly compatible with standard drift tube ion mobility mass spectrometers (DT-IMMS). Compared to previous FT-IMS experiments, our new approach requires only a single gate and circumvents the need for signal apodization by combining data from two frequency pulsing sequences 180° out of phase. Assessment of our initial results highlights an increase in signal-to-noise (SNR) relative to both previous implementations FT-IMS experiments and signal averaged (SA) experiments. For select tetraalkylammonium salts SNR improvements of more than one order of magnitude are routinely possible. To explore the performance metrics associated with the technique a number of experimental variables were systematically altered including frequency sweep range, sweep time, and data acquisition time. Using this experimental design we present the key aspects, considerations, and minimum resources necessary for other IMS researchers to incorporate this operational mode into their research. The two-phase FT-IMMS technique offers a tractable mechanism to enhance sensitivity for IMMS measurements and its broad-scale adoption by IMMS researchers promises to enhance the acquisition speed for mobility measurements using hybrid instrumentation.

Keywords: Ion Mobility Spectrometry; Mass Spectrometry; Fourier Transform; Multiplexing

1. Introduction

Finding heavy application in the field as an analytical tool, drift-tube ion mobility spectrometry (DT-IMS) is largely unmatched in its ability to rapidly screen passengers, cargo, and the surrounding environment for narcotics, explosives, and chemical warfare agents.[1-3] With strong ties to the fundamentals of gas-phase kinetic theory DT-IMS also finds utility as an informative tool to probe gas-phase ion chemistry, kinetics, and under select conditions gas-phase ion conformations.[4-8] Regardless of its intended application, the ability to rapidly resolve and detect ion populations remains paramount. However, as with many time-dispersive techniques challenges related to duty cycle are quite common for DT-IMS measurements. The duty cycle in most DT-IMS experiments are usually on the order of < 1% and this limitation in ion throughput naturally impacts sensitivity.[9, 10] Despite this limitation a suite of vendors have begun producing a range of mobility-based instruments, including DT-IMS systems, for the research community and this access has further propelled the adoption of the technique.[11-13] While these ion mobility-mass spectrometry (IMMS) instrument enable a broad class of researchers, they are still limited by duty cycle which constrains their ultimate potential. These classic trade-offs are by no means new problems but few solutions have been wholly adopted by the community.

The first explicit attempt at enhancing the duty cycle of DT-IMS was reported in 1985 by Knorr et al. through the inventive use of the Fourier transform.[14] By frequency modulating a set of ion gates located at the ends of a drift tube these researchers were able to produce an ion interferrogram that could be transformed into the time domain to extract mobility information. In subsequent publications stretching into the 2000's this

approach for standalone FT-IMS was demonstrated for a range of compound classes and was even employed as means to capture mobility data following chromatographic separations.[15-18] It should be noted, that while the FT-IMS method described by Knorr et al. was the first to directly employ the Fourier method to ion mobility systems, early work by Tyndall demonstrated a conceptually similar device for measurement mobility.[19, 20] Tyndall's experiment also frequency modulated a set of ion gates but these experiments were designed for considerably different reasons. Due to the lack of digital recording and modern current amplification electronics in the early 20th century modulating ion gates in the frequency domain effectively coupled comparatively high-speed gas-phase processes with more manual approaches to data acquisition.

Historically, FT-IMS experiments, though clearly an improvement over the SA approach, never realized the full SNR potential suggested by theory.[17, 21, 22] This observation was in large part due to the requirements of the signal processing routines used for the Fourier transform. More specifically, software and hardware implementations of the fast-Fourier transform (FFT) followed the classic Tukey Coolidge FFT approach that requires signal vector lengths that scale as a power of 2^n - 1.[23] An immediate byproduct of this approach combined with the Faraday plate detector using in the original FT-IMS experiment was a requirement to apply apodization functions to effectively reconstruct the ion signal in the drift time domain.[16, 17] Such functions have the unfortunate impact of drastically reducing the available signal intensity.[16]

The benefits of signal multiplexing significantly enhance a number of classical experiments routinely used in analytical chemistry.[24, 25] For example Fourier transform infrared spectroscopy and nuclear magnetic resonance (NMR) measurements all rely

heavily upon multiplexed approaches to signal acquisition. For more complex multidimensional NMR experiments Hadamard multiplexing also finds utility. As opposed to the Fourier transform mathematics which rely upon periodic functions (i.e. *sin* and *cos*), the Hadamard approach uses discrete on/off cycles to encode information.[17] First implemented in 2005, Hadamard transform IMS demonstrated significant gains over SA-IMS and these results prompted the rapid integration of this technique with hybrid ion mobility time-of-flight mass spectrometry measurements.[26-29] This mode of operation does not require any hardware specific modifications to implement and given the range of Hadamard sequences available is readily adapted to a range of drift tube ion mobility experiments. Though outside the scope of this discussion, other notable multiplexing approaches to IMS experiments include the use of modified pseudo-random sequences,[28, 30] Barker codes,[31] phase-modulated IMS,[32] and most recently overtone mobility spectrometry (OMS).[33, 34] In all cases, the primary focus is to enhance ion throughput and maximize signal to noise ratio for a technique that has historically be challenged by low duty-cycles.

Following the pioneering FT-IMS work by Knorr et al. we demonstrate for the first time a new Fourier-based approach to yielding mobility information from a drift-tube ion mobility system coupled with a TOF-MS. These initial experiments suggest Fourier transform IMMS (FT-IMMS) approaches are a highly tractable, require only a single ion gate, do not require apodization, and provide marked improvements in signal to noise ratio compared to signal averaging experiments. Additionally, our FT-IMMS technique does not suffer from the potentially detrimental artifacts observed for select forms of Hadamard IMS experiments.[27, 35, 36]

2. Experimental

2.1 Atmospheric Pressure Ion Mobility Time-of-Flight Mass Spectrometer

Fourier multiplexing experiments were conducted using a custom atmospheric pressure ion mobility system interfaced to a compact time of flight mass spectrometer (TOF-MS, TOFWERK, Thun, Switzerland). This instrument, based upon a stacked-ring drift tube design is capable of operation from ~100 to 250 °C with a homogeneous electric field of ~350 V/cm used in these experiments.[37] Counter-current flow of high-purity, dry nitrogen was introduced at the exit of the drift cell at ~1 L/min and atmospheric pressure (~690 Torr in Pullman, WA). Following ionization using an electrospray ionization source, ions traversed a short desolvation region (~10 cm) before encountering a Bradbury-Nielsen ion gate (BN-gate).[38] The circular BN-gate frame was constructed using two 99% alumina rings (50 mm ID x 58 mm OD x 3.5 mm thick) that served to hold two electrically isolated sets of parallel wires made of Alloy-46 (California Fine Wire Co., Grover Beach, CA). The wire was approximately 75 μm in diameter and the spacing of the BN-gate was 0.64 mm. The entire gate assembly was held together using a high temperature ceramic epoxy supplied from Cotronics (Resbond 940, Brooklyn, NY). The choice of materials for this BN-gate was guided by the desire to match the thermal coefficients of expansion to maintain gate integrity. Symmetric pulsing of the BN-gate (+/- 45 V) was accomplished using a custom floating power supply which enabled ions to enter the 23 cm-long drift tube connected to the TOF-MS. Serving as the detector, this mass spectrometer acquired full mass spectra (0-1200 *m/z*) in 60 μs for a sampling rate of 16,667 kHz. Signal averaging experiments utilized ion gate pulse widths ranging from

120-360 μs and ion mobility scan times of ~90 ms. Fourier transform spectra were obtained by sweeping the ion gate opening frequency from a minimum of 5 Hz up to a maximum of ~10 kHz. More specifically, the terminal frequencies examined in this effort were 2505, 5005, 7505, 8338, and 10,005 Hz. The time these pulsing sequences were swept varied between 1, 2, 4, and 8 seconds. While exact matching of experimental lengths between the FT-IMMS and SA-IMMS was not always possible, all efforts were made to acquire data in the respective modes that enabled relevant comparison with respect to the number of averages. The length of data acquisition for both the Fourier and SA-IMMS experiments was adjusted between 1, 2, 4, 5, and 8 minutes. Frequency scanning and waveform generation was accomplished using an Analog Discovery microcontroller (Digilent, Pullman, WA) capable executing a frequency sweep and delivering the pulsing sequence as a TTL-compatible signal. In addition to the frequency sweep this unit also contained the built-in capacity to alter the phase of the pulsing sequence.

2.2 Chemicals and Reagents

A range of tetraalkyimmonium salts (Sigma-Aldrich, St. Louis, MO) were used to evaluate the performance of the FT-IMMS technique relative to the signal averaging experiments. More specifically, the following salts were used throughout this study: tetrapropylammonium bromide (T_3A, *m/z* 130.1596), tetrabutylammonium bromide (T_4A, *m/z* 242.2848), tetrahexylammonium bromide (T_6A, *m/z* 354.4100), tetraheptylammonium bromide (T_7A, *m/z* 410.4726), tetraoctylammonium bromide (T_8A, *m/z* 466.5352), tetradecylammonium bromide ($T_{10}A$, *m/z* 578.6604), tetradodecylammonium chloride ($T_{12}A$, *m/z* 690.7856). A shorthand notation for each quaternary ammonium cation was

adopted with the number indicating the number of carbons in each side chain. Because only the cation was observed in the current study, the *m/z* listed for each analyte corresponds to the accurate mass of only that species and not the molecular weight of the full salt including the halide anion.

Used without any further treatment individual 50 μM solutions of these salts were made in a 50:50:0.1 mixture of acetonitrile, water, and formic acid (FA), respectively. From these stock solutions a mixture contain all of the quaternary ammonium salts was constructed with concentrations range from ~100 nM to 5 μM. This range was chosen to explore the ability of the system to capture information on analytes in mixtures of varying concentration. These samples diluted in 50:50:0.1 ACN:H_2O:FA were infused into the electrospray unit using syringe pump (KD Scientific,) at 3 μL/min held at ~2800 V above the entrance to the IMS desolvation region.

3 Results and Discussion

3.1 Pulse Design, Signal Processing, and Data Transformation

There are a number of excellent reviews on Fourier transformation and many that are tailored specifically to challenges in the chemical sciences.[25, 39] Building upon these fundamentals, we introduce a customized approached to data acquisition for FT-IMMS experiments designed to circumvent some of undesirable artifacts that arise in a standard FT-IMS experiment.

Because a discrete on/off cycling of the BN-gate(s) is necessary for the classic implementation of the FT-IMS experiment the basic windowing function used to recover data in the mobility domain was based upon the rectangular pulsing scheme used for

the gating function.[14] This direct treatment of the data prior to performing a Fourier transform often produces a range of ringing artifacts due to the discrete truncation of the signal.[16] To address such threats to signal recovery apodization functions have historically been applied when using the FT-IMS technique, however, these functions also discard real signal to minimize the contributions of transform noise. The experimental sequence used in this implementation of the FT-IMMS experiment is outlined in Figure 1. This figure only shows the first 200 ms of a frequency sweep ranging from 5-7505 Hz over the course of 2 seconds but serves to highlight the multi-step experimental process necessary to recover mobility spectra from the multiplexed experiment without apodization. Figure 1a corresponds to the linear frequency sweep applied to the BN gate and is denoted as the 0° pulsing sequence. This sequence initiates the experiment with the BN gate in the open configuration and proceeds through the frequency sweep with a 50% duty cycle. Using the TOF-MS as a detector the raw data in the time-domain were extracted based upon a specific range of *m/z* values. Figure 1b represents the raw, unsmoothed signal data for T_8A at *m/z* 466.5 that correspond to the 0° pulsing sequence (Figure 1a). It should be noted that a discrete transformation of these data result in an observable mobility peak but with significant ringing due to the truncation of the signal for the closed gating cycle (See Supplementary Information Figures S1-S3.). In many ways, the ideal time-domain signal approaches a free-induction decay (FID) similar to the spectral themes observed in NMR and Fourier transform ion cyclotron experiments. However, in order to achieve such a result for a FT-IMMS setup a complementary signal set is required. This result can be attained by operating the frequency sweep 180° out of phase relative to the initial pulsing sequence. Figure 1e outlines the pulse sequence

that accomplishes this goal relative to Figure 1a and it, too, produces a characteristic time-domain signal that when transformed produces signal ringing in the frequency domain. To avoid confusion, Figure 1d is derived from the application of the pulsing sequence shown in Figure 1e to show the algorithmic approach used to arrive at the combined signal shown in Figure 1c. The combined phase data represents a direct approach without apodization that effectively fills the gaps in the raw data that would otherwise be observed as zeros and establish the condition conducive to ringing upon transformation. In many ways this is direct means of efficiently simulating a second ion gate algorithmically.[21] When the raw data from the two-data are combined they result in a signal that largely adopts the shape of FID and is centered about 0. Figure 2 highlights such a result and represents the experimental scheme shown in Figure 1 but for T_6A and a sweep time of 4 s and a maximum frequency of 8338 Hz or ½ the frequency of the TOF-MS system acquisition rate.

Following the experimental steps outlined in Figure 1 raw mobility signals in the time domain may be constructed for each *m/z* similar to the spectrum shown in Figure 2. Though the main trace shown in Figure 2 has been smoothed using a binomial function only the raw data were used for SA-IMS comparison. These raw data and full FID for the T_6A are shown within the inset of Figure 2. The smoothed blue traces in Figure 2 are presented to highlight spectral features with all other traces (light red) corresponding to the raw signal.

Transitioning from the raw data shown in Figure 2 spectra to traditional DT-IMS may be constructed through the application of the fast Fourier transform (FFT). The FFT used to produce the transformed spectra in Figure 3 is a multidimensional prime factor

decomposition derivative of the Cooley-Tukey algorithm (IGOR Pro, Wavemetrics, Lake Oswego, OR). Positive trending peaks correspond to the FFT of the raw signal for each T_XA salt, whereas the negative trending peaks were obtained using the signal-averaging mode. The inversion of peaks was conducted only for presentation purposes and the stacked plot also aids in the visual inspection of the range and type of noise observed for each operational mode.

Before discussing the figures of merit related between the two modes of operation it is necessary to address the systematic frequency shift observed with the FT-IMMS experiment. Using a standard two-gate system to acquire FT-IMS data, the mechanism to recover drift time is achieved by dividing the experimentally measured frequency (i.e. result following FFT) by the sweep rate in Hz/s. This step produces a spectrum with peak locations that directly correspond to the IMS drift times simply because the two gate configuration explicitly defines the drift region. In the case of the FT-IMMS experiment using a TOF-MS there are additional, though comparatively small, contributions to the recorded time that correspond to ion flight times that are not governed by mobility. Typically ion transit times in the compact TOF-MS, including the *m/z* separation, are up to a few hundred microseconds. These contributions do not shift the overall drift time significantly but can contribute to the errors in mobility calculations. More importantly for the current work, was an apparent bias associated with the applied frequency sweep rate. All linear sweep experiments across 1, 2, 4 and 8 seconds exhibited a systematic bias towards larger frequencies upon transformation using the scheme outlined in Figure 1. Initial investigations of this behavior focused on aliasing effects, however, because the shift observed was toward higher frequency its origins are be-

lieved to arise from another highly deterministic error. It is worthy to note that systematic alteration of the gate pulsing voltage was explored but determined not to play a role in the observed frequency shift. By directly comparing the experimentally determined signal-averaged drift times with those measured using the FT-IMMS experiment a Person's coefficient of linearity (R^2) of 0.9983 was determined. Using this relationship the measured frequencies were shifted according to the apparent bias induced by the hardware employed in this work. Following this correction the average percentage deviation in observed drift times for the FT-IMMS was 0.020 +/- 0.77% compared to SA-IMMS experiments.

3.2 Evaluation of Transformed Signal to Noise Ratio

Compared to the historical approach to FT-IMS experiments, the scheme shown in Figure 1 requires the acquisition of two data sets prior to applying the FFT. Because this additional spectrum doubles the required experiment time, comparison to single phase FT-IMMS experiments must be adjusted by this factor. Figure 4 shows the result of three representative transformations for the T_6A signal including the 0°, 180°, and combined phase data sets. The SNR was calculated by measuring the standard deviation of the noise across a range expected to be absent of ions (i.e. 10-20 ms), multiplying this value by 3, and comparing this to the maximum signal intensity for a given peak. The SNR for the three different transforms shown in Figure 4 highlights the clear benefit afforded by the combining of the different phases. Another example demonstrating the benefits of the combined-phase approach additional figures may be found in the Supplementary Information (Figures S1-S3).

The SNR for the 0°, 180°, and combined signals were 69, 89, and 326 respectively. Based upon the principles of signal averaging doubling the experiment time to match the time required to produce the combined signal would maximally increase the SNR by a factor of √2. Even for the best SNR result from a signal phase FT-IMMS experiment this only leads to a maximum SNR of 125 which differs from the combined phase approach by more than a factor of 2.5. Another interesting, yet unexploited, feature in the datasets shown are the periodic signals also found in the noise. Closer examination of the spectral regions that do not contain well-defined mobility peaks (i.e. inset of Figure 4) highlight the appearance of a cyclical noise component that corresponds directly to 120 Hz noise. It has been our observation that the combined phase aids in reducing this noise component because the times at which each phase of the experiment are initiated differ. The increase in overall SNR observed for the combined-phase FT-IMMS approach is derived from the increased number of resonant ion beats observed at the detector. Another interesting aspect of the combined approach is the small, yet consistent, shift in the drift times between the individual and combined phase results. The combined phase transform yields a peak centroid that is always between the value observed for 0° and 180° transformed results. Though a minor correction, the combined phase approach may aid in a more accurate reflection of drift time using FT-IMMS approaches.

Using the approach to calculating SNR for Figure 4 the SNR for T_4A, T_8A, and $T_{12}A$ across a range of frequencies and sweep times is shown in Figure 5. A full accounting of SNRs for all of the T_XA ions may be found in the Supplementary Information. Figure 5 captures the SNRs observed for each of the target T_XAs as a function

of both sweep range and time and for comparison equivalent SA-IMMS SNRs are shown as a subplot. To minimize the impact of differing averages, all of the data in Figure 5 were acquired for 2 minutes and the SA-IMMS data sets originated from experiments using a 240 μs gate pulse width and 90 ms scan times. In all combinations of sweep times and frequency ranges the FT-IMMS experiments yielded SNRs that exceeded the SA-IMMS data sets. For the extended sweep times (i.e. 8 seconds) even with the same 2 minute acquisition time, the SNR gain for the FT-IMMS experiments were often an order of magnitude greater than the signal averaged data. However, this trend was not always true for the $T_{12}A$ species which did not exhibit as large SNR gains for higher sweep frequencies. This again is attributed to the reduced numbers of resonant ion beats that are observed in the raw data sets because a shorter amount of time is spent on the resonant frequencies for faster sweep times. There may be a temptation to interpret the observed changes in SNR as a function of *m/z*, however, the absolute concentrations of the different species were chosen to compensate for differences in ionization efficiencies. Long sweep times and lower terminal frequencies produced the largest SNR gains, however as Figure 6 illustrates reduced frequency ranges rarely yield spectra with the highest resolving power. Though outside the scope of this current investigation the changes in SNR for the same T_XAs as a function of sweep time and frequency highlight a potential challenge for obtaining quantitative data. This issue and others are the focus of a separate investigation.

3.3 Evaluation of Multiplexed Resolving Power

Figure 6 provides a resolving power (Rp) comparison between the different

modes of analyses for 3 representative T_XAs (T_4A, T_8A, and T_{12}A). Only a subset of the data are shown here for discussion purposes and the full distilled data for all of the T_XA salts may be found in the Supplementary Information. As with the SNR comparison, the frequency sweep range and time influences the resulting mobility spectra and it was for this reason that Rp of each spectrum was plotted as a function of sweep rate (Hz/s). The colored markers highlight data from the FT-IMMS data while the black dashed lined corresponds to the SA-IMMS data. This latter plot highlights a general trend that SA-IMMS data provided modestly higher resolving powers than the multiplexed modes but a more detailed examination of the data illustrate a more complex relationship for the FT-IMMS experiments. Because these data are plotted as a function of sweep rate there are FT-IMMS results that were acquired using the same frequency range but result in data points at the extremes of the axes shown. For example a spectrum resulting from a 10 kHz sweep over 1 second yield FT-IMMS data points that are located to the far right of each plot while the same frequency range swept for 8 seconds produce data points with an x-axis value of 1250 Hz/s. Using Figures 1 and 2 as reference, the fidelity of the IMS peak from each frequency sweep is largely due to the number of resonant ion beats that are accurately recorded during the experiment. For high sweep rates the time the ion gate is cycling at any given frequency is shortened which in turn reduces the number of resonant ion packets that are available. It is this trade-off that produces the characteristic decline in FT-IMMS resolving power at higher sweep rates. It is worthy to note that in all cases shown in Figure 6 the highest resolving power for the FT-IMMS spectra were obtained for 8 second sweep times while the lowest resolving power was generally obtained for 1 second sweep times--this result is in direct contrast to the SNR

result which again highlights the trade-off inherent in this technique.

Another relevant comparison between the SA-IMMS and FT-IMMS is the degree to which each approaches the theoretical resolving power predicted by a standard application of diffusion rates. This conditional resolving power (R_c) may be determined as outlined in references 39 and 40 but is based upon the experimental conditions used to acquire DT-IMS data.[40, 41] For the SA-IMMS data shown in Figure 6 the R_c for T_4A, T_8A, and $T_{12}A$ were 93, 105, and 109 respectively. These values were calculated using values of 690 Torr, 493 Kelvin, 250 V/cm and a 240 μs gate pulse width, and the reported reduced mobilities for the target T_XA salts. For the T_4A ion the measured resolving power reached 98% of the theoretical maximum (i.e. R_c) while the $T_{12}A$ species only reached 87% of the theoretical maximum for that species. The approach calculating R_c for the FT-IMMS experiment is directly related to the maximum frequency swept.[14] For example, frequency sweeps that end at 10 kHz results in a BN gate 50% duty cycle that alternates between on and off states every 100 μs. Alternatively, conditional resolving power estimations for a FT-IMMS experiments terminating at 4,167 Hz would be equivalent to a SA-IMMS experiment using a 240 μs gate pulse width. While that specific frequency was not chosen for the FT-IMMS experiments, the outlined here data were acquired for terminal frequencies of 5005 Hz. For those FT-IMMS data sets (equivalent to 200 μs SA-IMMS experiments) the experimentally observed resolving powers achieved between 86 and 98 % of the predicted R_c values. This range is due to a number of factors including the speed at which ions traverse the ion gating region and the depletion of the ion population that occurs as the ion gate returns to the closed state. The ion gate modeling and experimental work recently outlined by Puton et al. highlights the impacts

of different gating schemes on the ion population entering the drift cell.[42, 43] The combined impacts of gate depletion and the increasing frequency of ion gating cycling establish conditions for the decay of the FT-IMMS signal. This behavior is not entirely surprising but also sets the stage for the inverse transform necessary to recover the original IMS peak. Another factor that also contributes to some of this resolving power variability is the use of a time-to-digital converter rather than an analog-based acquisition system. Again it should be reiterated that the maximum Rp for the FT-IMMS experiments was for the 8 seconds sweep times and it is our assertion that this observation is due to the increased numbers of resonance ion beats that may be observed for longer sweep times. This final observation regarding resolving power is based upon a general trend of increasing resolving power with decreasing analyte drift time (data not shown). Stated differently, higher FT-IMMS resolving powers were observed for ions with higher mobilities (shorter drift times) regardless of the frequency range swept.

4. Conclusions

By modulating an ion beam in an ion mobility time of flight system using two frequency chirps oriented 180° out of phase we have demonstrated a new FT-IMMS approach that enhances both SNR, ion throughput, and does not require any hardware modifications. Initial evaluations of the FT-IMS approach illustrated modest gains in signal-to-noise ratio (SNR) when compared to signal-averaged IMS experiments (SA-IMS) with maximum realized gain factors of ~3.[14, 17] The inability of previous systems to fully realize multiplexing gains is attributed to a number of factors including the need for two physical ion gates and most importantly the need for apodization function to recover

IMS spectra from raw frequency-encoded ion signals.[16] In contrast, the two-phase FT-IMMS technique we outline is compatible with only a single ion gate and requires no apodization functions to reconstruct drift time. This latter benefit is a direct result of combining the data from the two respective pulsing phases. Because a wide range of factors was explored in this effort including frequency range, frequency sweep time, and data acquisition time an explicit SNR gain attributed to the FT-IMMS technique is difficult to deduce. However, without any advanced signal processing steps (e.g. smoothing or matched filtering) it is possible to realize SNR gains that approach an order of magnitude for the FT-IMMS technique compared to the traditional signal averaged mode of operation. Larger SNR gains are possible, however, these are for FT-IMMS pulse modes yield lower resolution ion mobility spectra. In summary, the SNR gains afforded by the two-phase FT-IMMS approach are readily achievable using any standard DT-IMMS and the ultimate performances is only limited by the maximum frequency at which the ion gate may operate effectively and the sampling rate of the detector.

Figure Captions

Figure 1. FT-IMMS multiplexing scheme that combines the raw time-domain data ((b) and (d)) from two different pulsing schemes that are 180° out of phase ((a) and (e)). This experimental sequence is followed to obtain a raw combined phase spectrum (c) suitable for transformation into the frequency domain which contains mobility data. By combining the two signal traces originating from the two pulse phases transform artifacts are greatly minimized.

Figure 2. Combined phase time domain data resulting from the scheme outlined in Figure 1. The data in the main figure correspond to data extracted for the T_6A ion (m/z 354) with only the first 400 ms being shown. The total frequency sweep time for these data were 4 seconds and these data are shown in the top right inset. For display purposes the blue traces in this figure were smoothed using a 25 point binomial function, while the semi-transparent red trace corresponds to the raw data. For all transformed data and comparisons shown in this manuscript only raw, unsmoothed data were used.

Figure 3. Direct spectral comparison between FT-IMMS experiments and SA-IMMS data for all of the T_XA salts examined. Positively oriented peaks correspond to the FT-IMMS experiment while the inverted peaks originate from the signal-averaged experiment (240 µs gate pulse width). These data illustrate the improved signal to noise ratios afforded by the FT-IMMS technique. Though many different parameters may be adjusted for the FT-IMMS experiment the data provided in this figure were derived for a 4 second sweep spanning 8338 Hz.

Figure 4. While possible to transform the raw data from individual signal chirps the combined phase data show a marked improvement in signal to noise ratio even when doubling the acquisition time for a single phase. Transformed data for each individual phase and their combination are shown. The inset shown for longer times highlights the common noise characteristics observed including the periodic contributions from 120 Hz noise.

Figure 5. Impact of sweep time and frequency range on signal to noise ratio (SNR) for 3 of the 9 T_XA salts examined. For comparison the figure inset provides the SNR observed for the SA-IMMS data. Maximum FT-IMMS SNR was observed from longer sweep times which is directly related to the number of well-resolved resonant ion beats found in the raw data.

Figure 6. Resolving power comparison between different experimental variables for the FT-IMMS experiment. For the 3 T_XAs shown (T_4A, T_8A, and $T_{12}A$) the signal averaged resolving power is highlighted as a straight horizontal line. Shorter frequency ranges and sweep times yielded the lowest resolving power for the FT-IMMS experiment. Resolving powers that exceeded the SA-IMMS data were routinely observed for broader frequency sweeps and sweep times of 8 seconds.

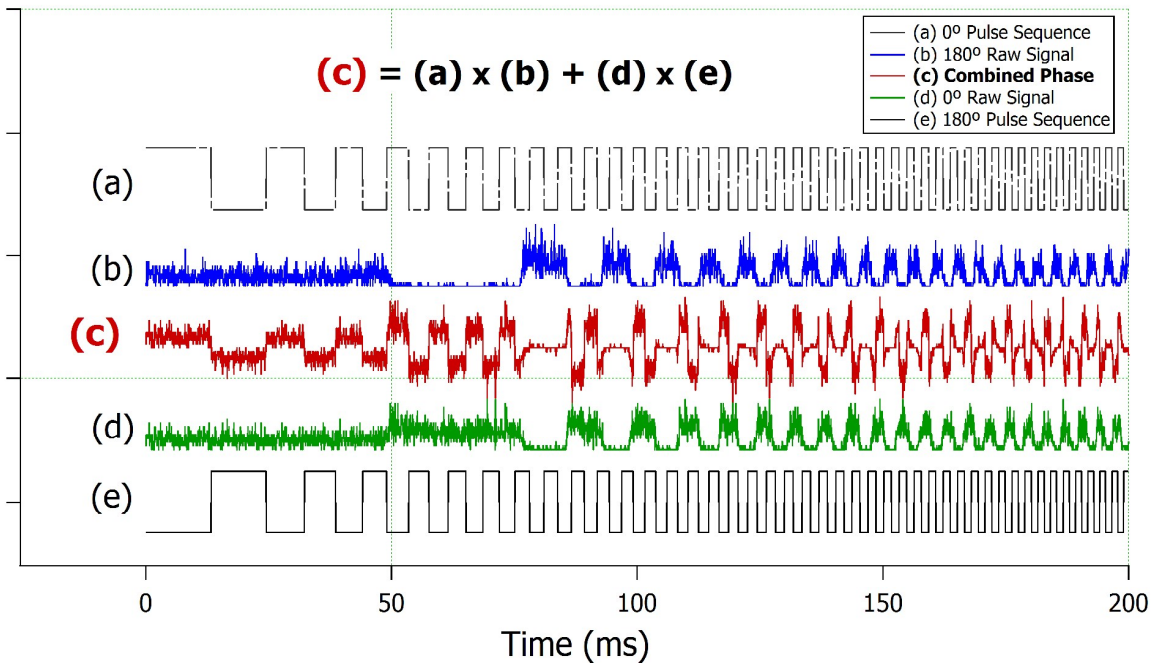

Figure 1. FT-IMMS multiplexing scheme that combines the raw time-domain data ((b) and (d)) from two different pulsing schemes that are 180° out of phase ((a) and (e)). This experimental sequence is followed to obtain a raw combined phase spectrum (c) suitable for transformation into the frequency domain which contains mobility data. By combining the two signal traces originating from the two pulse phases transform artifacts are greatly minimized.

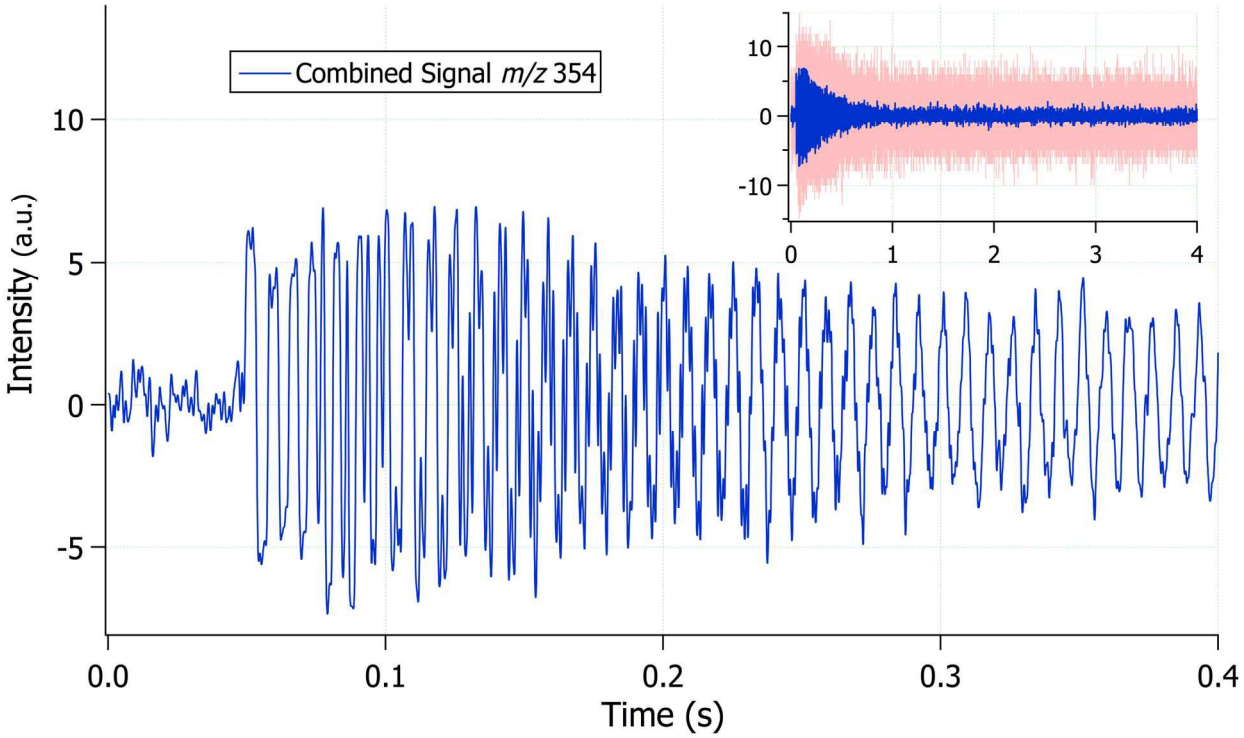

Figure 2. Combined phase time domain data resulting from the scheme outlined in Figure 1. The data in the main figure correspond to data extracted for the T_6A ion (m/z 354) with only the first 400 ms being shown. The total frequency sweep time for these data were 4 seconds and these data are shown in the top right inset. For display purposes the blue traces in this figure were smoothed using a 25 point binomial function, while the semi-transparent red trace corresponds to the raw data. For all transformed data and comparisons shown in this manuscript only raw, unsmoothed data were used.

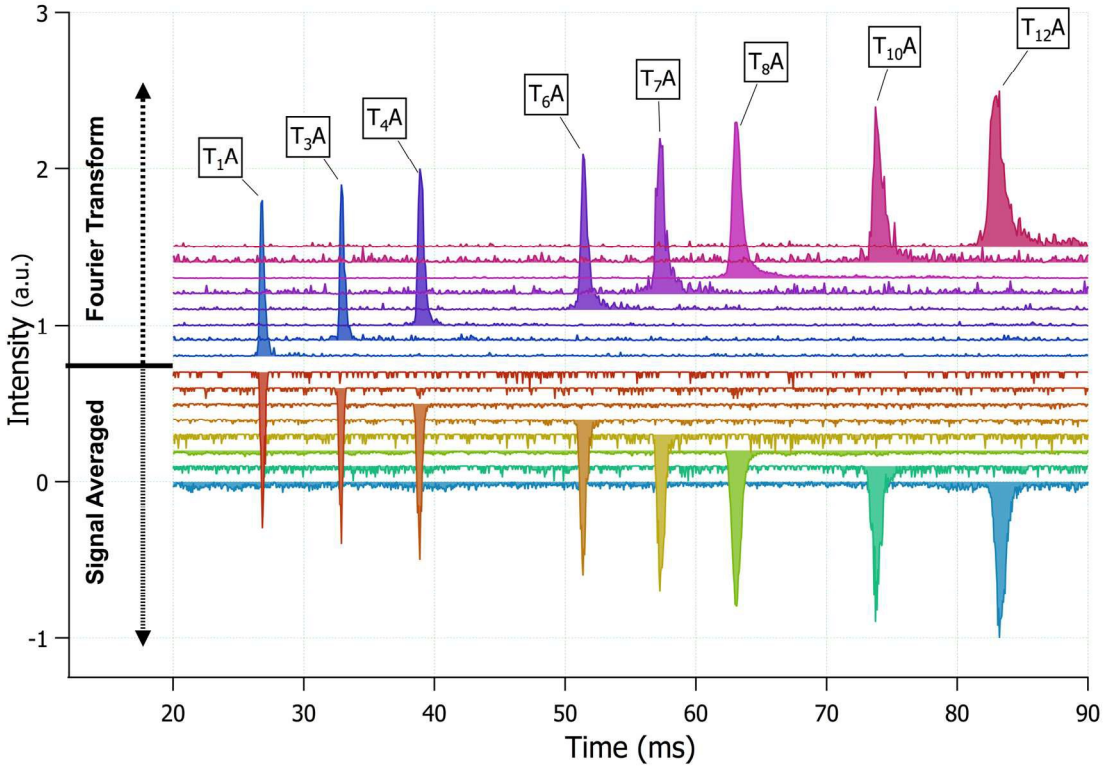

Figure 3. Direct spectral comparison between FT-IMMS experiments and SA-IMMS data for all of the T_XA salts examined. Positively oriented peaks correspond to the FT-IMMS experiment while the inverted peaks originate from the signal-averaged experiment (240 μs gate pulse width). These data illustrate the improved signal to noise ratios afforded by the FT-IMMS technique. Though many different parameters may be adjusted for the FT-IMMS experiment the data provided in this figure were derived for a 4 second sweep spanning 8338 Hz.

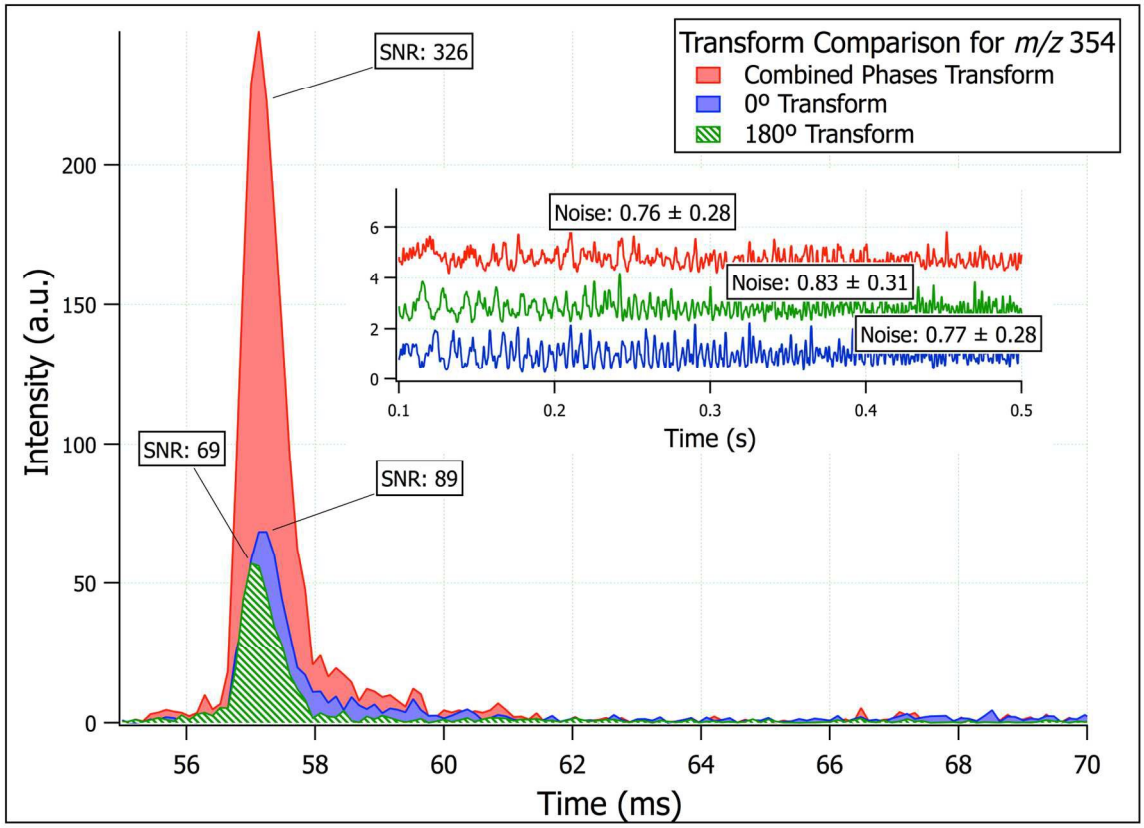

Figure 4. While possible to transform the raw data from individual signal chirps the combined phase data show a marked improvement in signal to noise ratio even when doubling the acquisition time for a single phase. Transformed data for each individual phase and their combination are shown. The inset shown for longer times highlights the common noise characteristics observed including the periodic contributions from 120 Hz noise.

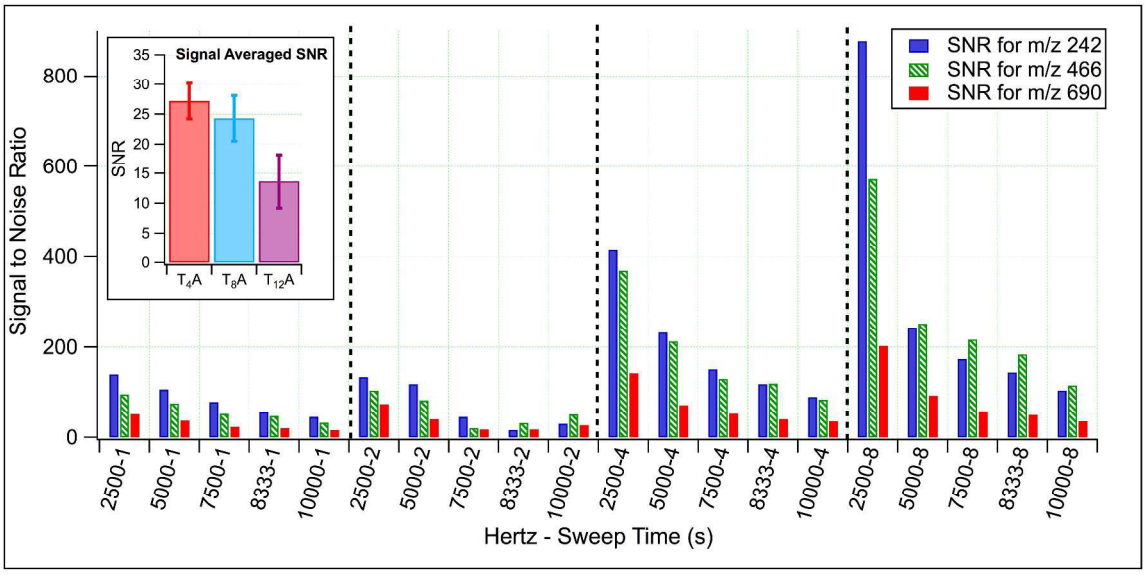

Figure 5. Impact of sweep time and frequency range on signal to noise ratio (SNR) for 3 of the 9 T_XA salts examined. For comparison the figure inset provides the SNR observed for the SA-IMMS data. Maximum FT-IMMS SNR was observed from longer sweep times which is directly related to the number of well-resolved resonant ion beats found in the raw data.

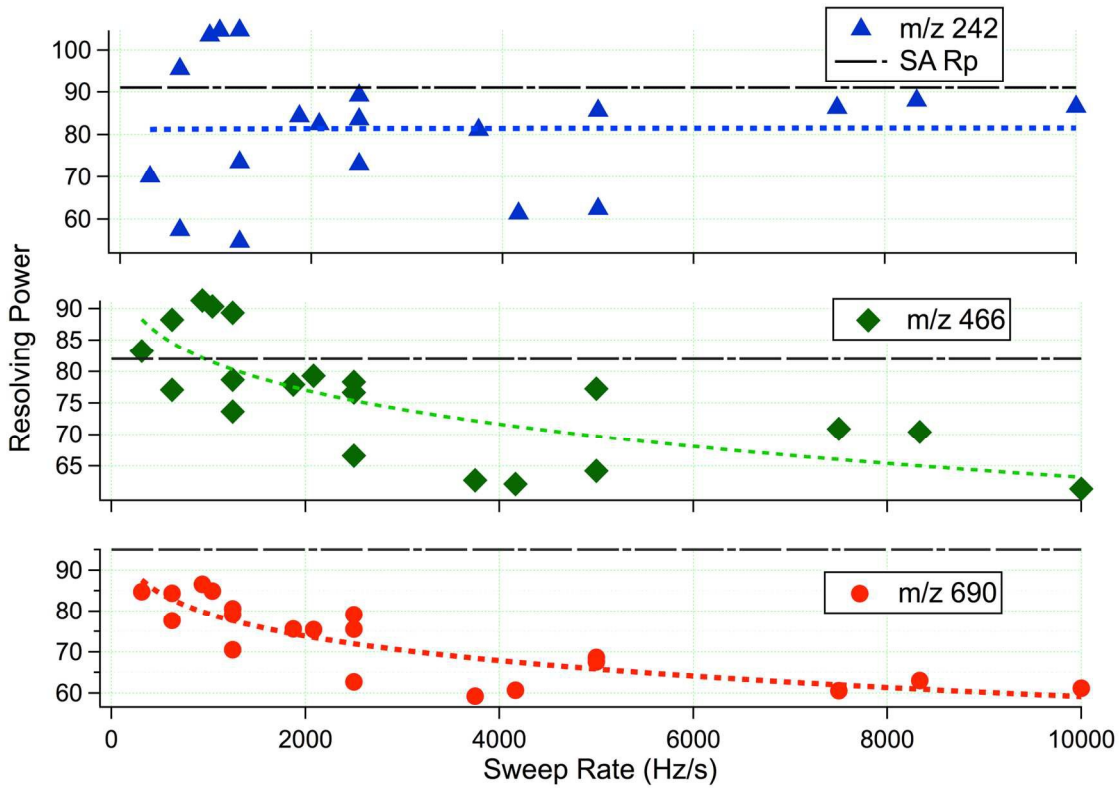

Figure 6. Resolving power comparison between different experimental variables for the FT-IMMS experiment. For the 3 T_XAs shown (T_4A, T_8A, and T_{12}A) the signal averaged resolving power is highlighted as a straight horizontal line. Shorter frequency ranges and sweep times yielded the lowest resolving power for the FT-IMMS experiment. Resolving powers that exceeded the SA-IMMS data were routinely observed for broader frequency sweeps and sweep times of 8 seconds.

References

1. R. G. Ewing, D. A. Atkinson, G. Eiceman and G. Ewing, *Talanta*, 2001, **54**, 515-529.
2. W. E. Steiner, B. H. Clowers, L. M. Matz, W. F. Siems and H. H. Hill, *Analytical chemistry*, 2002, **74**, 4343-4352.
3. G. Eiceman and J. Stone, *Analytical chemistry*, 2004, **76**, 390 A-397 A.
4. M. Tabrizchi and S. Shooshtari, 2003, **35**, 863-870.
5. R. G. Ewing, G. A. Eiceman and J. Stone, *International Journal of mass spectrometry*, 1999, **193**, 57-68.
6. T. Wyttenbach and M. T. Bowers, in *Modern Mass Spectrometry*, Springer, 2003, pp. 207-232.
7. J. L. Benesch, B. T. Ruotolo, D. A. Simmons and C. V. Robinson, *Chemical reviews*, 2007, **107**, 3544-3567.
8. H. Shi, N. Atlasevich, S. I. Merenbloom and D. E. Clemmer, *Journal of The American Society for Mass Spectrometry*, 2014, **25**, 2000-2008.
9. S. C. Henderson, S. J. Valentine, A. E. Counterman and D. E. Clemmer, *Analytical chemistry*, 1999, **71**, 291-301.
10. B. H. Clowers, Y. M. Ibrahim, D. C. Prior, W. F. Danielson, M. E. Belov and R. D. Smith, *Analytical chemistry*, 2008, **80**, 612-623.
11. C. K. Hilton, C. A. Krueger, A. J. Midey, M. Osgood, J. Wu and C. Wu, *International Journal of Mass Spectrometry*, 2010, **298**, 64-71.
12. J. C. May, C. R. Goodwin, N. M. Lareau, K. L. Leaptrot, C. B. Morris, R. T. Kurulugama, A. Mordehai, C. Klein, W. Barry and E. Darland, *Analytical chemistry*, 2014, **86**, 2107-2116.
13. S. D. Pringle, K. Giles, J. L. Wildgoose, J. P. Williams, S. E. Slade, K. Thalassinos, R. H. Bateman, M. T. Bowers and J. H. Scrivens, *International Journal of Mass Spectrometry*, 2007, **261**, 1-12.
14. F. J. Knorr, R. L. Eatherton, W. F. Siems and H. H. Hill, *Analytical Chemistry*, 1985, **57**, 402-406.
15. R. L. Eatherton, M. a. Morrissey and H. H. Hill, *Analytical Chemistry*, 1988, **60**, 2240-2243.
16. R. H. S. Louis, W. F. Siems and H. H. Hill, 2000, 171-177.
17. Y. H. Chen, W. F. Siems and H. H. H. Jr, 1996.
18. R. Dietiker, F. Lena and P. Chen, 2007, 2796-2802.
19. A. M. Tyndall and G. C. Grindley, *Proceedings of the Royal Society of London*, 1926, **110**, 358-364.
20. A. M. Tyndall and L. R. Phillips, *Proceedings of the Royal Society of London*, 1926, **111**, 577-591.
21. E. Tarver, J. F. Stamps, R. T. Jennings and W. F. Siems, *International Journal for Ion Mobility Spectrometry*, 2000, **1**, 57-59.
22. E. E. Tarver, 2004, 1-13.
23. J. W. Cooley and J. W. Tukey, *Mathematics of computation*, 1965, **19**, 297-301.
24. L. Glasser, *Journal of Chemical Education*, 1987, **64**, A260.
25. A. Marshall, *Fourier, Hadamard, and Hilbert transforms in chemistry*, Springer Science & Business Media, 1982.

26. B. H. Clowers, W. F. Siems, H. H. Hill and S. M. Massick, *Analytical chemistry*, 2006, **78**, 44-51.
27. M. E. Belov, B. H. Clowers, D. C. Prior, W. F. Danielson III, A. V. Liyu, B. O. Petritis and R. D. Smith, *Analytical chemistry*, 2008, **80**, 5873-5883.
28. B. H. Clowers, M. E. Belov, D. C. Prior, W. F. Danielson, Y. Ibrahim and R. D. Smith, *Analytical chemistry*, 2008, **80**, 2464-2473.
29. A. W. Szumlas, S. J. Ray and G. M. Hieftje, *Analytical chemistry*, 2006, **78**, 4474-4481.
30. G. A. Harris, M. Kwasnik and F. M. Fernández, *Analytical chemistry*, 2011, **83**, 1908-1915.
31. K. B. Pfeifer and S. B. Rohde, *Sensors Journal, IEEE*, 2007, **7**, 1130-1137.
32. A. W. Szumlas and G. M. Hieftje, *Analytica Chimica Acta*, 2006, **566**, 45-54.
33. S. Lee, M. a. Ewing, F. M. Nachtigall, R. T. Kurulugama, S. J. Valentine and D. E. Clemmer, *The journal of physical chemistry. B*, 2010, **114**, 12406-12415.
34. R. T. Kurulugama, F. M. Nachtigall, S. Lee, S. J. Valentine and D. E. Clemmer, *Journal of the American Society for Mass Spectrometry*, 2009, **20**, 729-737.
35. N. Sloane, M. Harwit and M.-H. Tai, *Applied optics*, 1978, **17**, 2991-3002.
36. S. A. Prost, K. L. Crowell, E. S. Baker, Y. M. Ibrahim, B. H. Clowers, M. E. Monroe, G. A. Anderson, R. D. Smith and S. H. Payne, *Journal of The American Society for Mass Spectrometry*, 2014, **25**, 2020-2027.
37. K. M. Roscioli, X. Zhang, S. X. Li, G. H. Goetz, G. Cheng, Z. Zhang, W. F. Siems and H. H. Hill, *International Journal of Mass Spectrometry*, 2013, **336**, 27-36.
38. C. Wu, W. F. Siems, G. R. Asbury and H. H. Hill, *Analytical chemistry*, 1998, **70**, 4929-4938.
39. O. Trapp, *Angewandte Chemie International Edition*, 2007, **46**, 5609-5613.
40. E. J. Davis, M. D. Williams, W. F. Siems and H. H. Hill Jr, *Analytical chemistry*, 2011, **83**, 1260-1267.
41. J. C. May and D. H. Russell, *Journal of the American Society for Mass Spectrometry*, 2011, **22**, 1134-1145.
42. J. Puton, A. Knap and B. Siodłowski, *Sensors and Actuators B: Chemical*, 2008, **135**, 116-121.
43. F. K. Tadjimukhamedov, J. Puton, J. A. Stone and G. A. Eiceman, *Review of Scientific Instruments*, 2009, **80**, 103103.